

An energy-efficient learning solution for the Agile Earth Observation Satellite Scheduling Problem

Antonio M. Mercado-Martínez, Beatriz Soret *Senior Member, IEEE*, Antonio Jurado-Navas *Member, IEEE*

Abstract—The Agile Earth Observation Satellite Scheduling Problem (AEOSSP) entails finding the subset of observation targets to be scheduled along the satellite’s orbit while meeting operational constraints of time, energy and memory. The problem of deciding *what* and *when* to observe is inherently complex, and becomes even more challenging when considering several issues that compromise the quality of the captured images, such as cloud occlusion, atmospheric turbulence, and image resolution. This paper presents a Deep Reinforcement Learning (DRL) approach for addressing the AEOSSP with time-dependent profits, integrating these three factors to optimize the use of energy and memory resources. The proposed method involves a dual decision-making process: selecting the sequence of targets and determining the optimal observation time for each. Our results demonstrate that the proposed algorithm reduces the capture of images that fail to meet quality requirements by $> 60\%$ and consequently decreases energy waste from attitude maneuvers by up to 78% , all while maintaining strong observation performance.

I. INTRODUCTION

One of the most relevant advances in the realm of Earth Observation (EO) has been the introduction of Agile Earth Observation Satellites (AEOS) [1]. Unlike Conventional Earth Observation Satellites (CEOS), which can only adjust their attitude along the roll axis, AEOS have a strong attitude adjustment capability along three axes (roll, pitch, and yaw). This allows AEOS to have longer Visible Time Windows (VTW), enabling multiple Observation Time Windows (OTW) for a single target. The VTW represents the time interval in which a concrete observation target can be observed, while the OTW represents its real observation time. Although this provides a wide range of options, it also complicates the selection of the OTW when multiple observation targets are involved in the same observation period, which is known as the Agile Earth Observation Satellite Scheduling Problem (AEOSSP). In particular, the AEOSSP consists of maximizing the total observation profit while satisfying all temporal, energy, and memory constraints. Such observation profit can be defined in different ways depending on the nature of the application.

However, this process is not always straightforward, as various factors impact the quality and, consequently, the usability of the collected images. For example, a substantial number of collected EO images are discarded because of cloud occlusion

[2]. Likewise, the presence of turbulence in the atmosphere causes aberrations in the image during its capture [3], which also results in its exclusion. Finally, image resolution must be also considered as some applications require high-resolution images to perform properly. This is defined by the ground sample distance (GSD), i.e., the real distance represented by a pixel in the image, which increases as the target moves away from the nadir. The smaller the GSD, the higher the image quality [4]. Nevertheless, the scope of AEOS allows us to integrate these factors into the AEOSSP, improving the performance and the obtained observation profit.

In this paper, we investigate a Deep Reinforcement Learning (DRL) [5] approach for solving the AEOSSP with time-dependent profits for a single AEOS taking into account the presence of clouds and atmospheric turbulence, as well as image resolution, in order to achieve both good energy and memory resources management. This involves a dual decision-making process, as it requires selecting both the sequence of targets and the best observation time for each. To address it, we model the problem as a graph and leverage the use of Graph Neural Networks (GNN).

The rest of the paper is organized as follows. Section II provides an overview of related works. In Section III, we introduce the system model. The optimization problem is described in Section IV, while the proposed algorithm is presented in Section V. The conducted experiments and the obtained results are discussed in Section VI, whereas Section VII concludes the paper.

II. STATE OF THE ART

The AEOSSP has been widely studied in recent years. Existing approaches can be classified into exact methods, heuristics, metaheuristics, and machine learning. Among machine learning methods, some studies have employed DRL, such as in the case of [6], where GNN were applied with promising results. This approach is particularly well suited to the problem, as it can be effectively modeled as a graph, a quite common practice in the field [7].

Cloud coverage remains a significant challenge within the scope of AEOSSP [7]. Various studies have addressed this issue, such as [2], where a re-scheduling algorithm based on cloud coverage forecasting was developed. On the other hand, the presence of atmospheric turbulence has not been as extensively explored in the AEOSSP context. However, [8] evaluates its impact on EO images and concludes that it is an important factor to consider.

Finally, image resolution is another critical aspect affecting

This work is funded by the Spanish Ministerio de Ciencia, Innovación y Universidades (project "TATOOINE", grant no. PID2022-136269OB-I00). The author thankfully acknowledges the computer resources, technical expertise and assistance provided by the SCBI (Supercomputing and Bioinformatics) center of the University of Malaga.

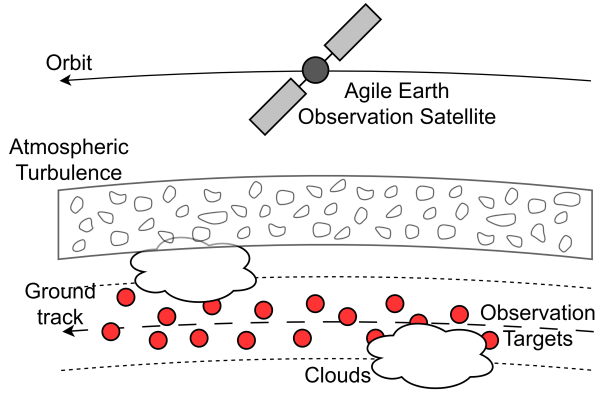


Fig. 1: Scenario with a single AEOS, multiple observation targets and the presence of clouds and atmospheric turbulence.

the quality of EO images. This factor was taken into account in [9], where an exact method for solving the AEOSSP with time-dependent profits was developed. There, the observation profit was formulated as a function of image resolution. Similar to our approach, this study incorporates a dual decision-making process that involves selecting the sequence of targets and determining the observation time for each.

III. SYSTEM MODEL

Fig. 1 shows the considered scenario consisting of an AEOS that observes a set of N ground observation targets along its orbit. The satellite operates at an altitude h_{sat} in an orbit with an inclination ζ , observing a set of targets T distributed within an observation area. Each target i represents a squared area of size l_{target} , which can be observed at $t_{i,n}$.

The attitude of the satellite during observation at $t_{i,n}$ is defined by the roll ($\theta_{i,n}$), pitch ($\phi_{i,n}$), and yaw ($\psi_{i,n}$) angles. The satellite's attitude maneuver capability is determined by its maximum roll, pitch, and yaw angles (θ_{max} , ϕ_{max} , and ψ_{max} , respectively) as well as the attitude transition time. These factors dictate which targets can be observed and scheduled at any given time. The attitude transition time is described by a piecewise linear function that depends on the speed of the camera and the angular difference between two consecutive observations [10]. Specifically, for the scenario where target i is observed at $t_{i,n}$ and target j is observed at $t_{j,m}$, the attitude transition time is defined as follows:

$$\Delta t_{i,n-j,m} = \begin{cases} 11.66, & \alpha_{i,n-j,m} \leq 10^\circ \\ 5 + \alpha_{i,n-j,m}/1.5, & 10^\circ < \alpha_{i,n-j,m} \leq 30^\circ \\ 10 + \alpha_{i,n-j,m}/2, & 30^\circ < \alpha_{i,n-j,m} \leq 60^\circ \\ 16 + \alpha_{i,n-j,m}/2.5, & 60^\circ < \alpha_{i,n-j,m} \leq 90^\circ \\ 22 + \alpha_{i,n-j,m}/3, & \alpha_{i,n-j,m} > 90^\circ \end{cases}, \quad (1)$$

$$\alpha_{i,n-j,m} = |\theta_{i,n} - \theta_{j,m}| + |\phi_{i,n} - \phi_{j,m}| + |\psi_{i,n} - \psi_{j,m}|, \quad (2)$$

where $\alpha_{i,n-j,m}$ is the total attitude transition angle between target i observed at $t_{i,n}$ and target j observed at $t_{j,m}$,

Clouds are modeled as a grid deployed at altitude h_{clouds} above the observation area. Each cell in the grid represents a square area of size l_{clouds} centered at a specific coordinate,

and is assigned a binary variable indicating the presence or absence of clouds in that area. P_{clouds} denotes the percentage of cells representing the presence of clouds within the grid. Cells representing cloud presence are grouped into clusters of adjacent cells, with each cluster emulating an individual cloud. $\delta_{i,n}$ represents the fraction of the target's surface covered by clouds when capturing target i at $t_{i,n}$.

Atmospheric turbulence is determined by the refractive index structure parameter C_n^2 , which is a statistical measure of the strength of the turbulence in the atmosphere, and, similarly to clouds, it is modeled as a grid deployed at altitude $h_{C_n^2}$ above the observation area. Each cell in the grid represents a square area of size $l_{C_n^2}$ centered at a specific coordinate, and is assigned a C_n^2 value. $P_{C_n^2, max}$ denotes the percentage of cells with a C_n^2 value greater than $C_{n, max}^2$ in the grid, with $C_{n, max}^2$ being the maximum allowed C_n^2 for obtaining a high-quality image. Since the channel characteristics determining C_n^2 values vary by position and are independent, the value of each cell is uncorrelated with the others. $C_n^2(i, n)$ represents the C_n^2 value affecting the image quality when capturing target i at $t_{i,n}$.

Both, $C_n^2(i, n)$ and $\delta_{i,n}$ values determine whether meteorological conditions for observing target i at $t_{i,n}$ are suitable for capturing the image. This suitability is represented by the following binary function:

$$f_{i,n}(C_n^2(i, n), \delta_{i,n}) = \begin{cases} 1, & C_n^2(i, n) \leq C_{n, max}^2 \\ & \text{and } \delta_{i,n} < \delta_{max} \\ 0, & \text{otherwise} \end{cases}, \quad (3)$$

where δ_{max} is the maximum permissible fraction of the target's surface that can be covered by clouds. If $f_{i,n}(C_n^2(i, n), \delta_{i,n}) = 1$, the conditions are deemed suitable; otherwise, $f_{i,n}(C_n^2(i, n), \delta_{i,n}) = 0$.

The AEOSSP to be formulated in this scenario is a dual decision-making problem involving the selection of the sequence of targets and determining the capture time for each. To address this, the system is modeled as a directed graph $G = (V, E)$, where V represents the set of nodes in the graph and E denotes the set of edges connecting them. Each node $v_{i,n}$ denotes a feasible pair observation target i at a capture time n , referred to as an action; and the edges $e_{i,n-j,m}$ connect nodes that can be scheduled in the same sequence while meeting the constraints. The graph also includes a node representing the last action taken, as well as a virtual node at the beginning of the observation which connects to all other nodes.

The information gathered at each node $v_{i,n}$ in the graph includes: the GSD of target i at $t_{i,n}$; $f_{i,n}(C_n^2(i, n), \delta_{i,n})$, representing the suitability of meteorological conditions when capturing target i at $t_{i,n}$; and the capture time $t_{i,n}$. Thus, we form the node features vector $\vec{v}_{i,n} = (GSD_{i,n}, f_{i,n}(C_n^2(i, n), \delta_{i,n}), t_{i,n})$. It is assumed that this information is available and can be processed to create the graph.

IV. AGILE EARTH OBSERVATION SATELLITE SCHEDULING PROBLEM

The AEOSSP consists of maximizing the total observation profit while meeting temporal, energy, and memory operational constraints. For the sake of simplicity, we have only considered time constraints. Interestingly, this results in significant energy and memory savings, as an optimal resolution of the AEOSSP leads to a better resource management, as later shown in the results. The mathematical formulation is as follows:

$$\max \sum_{i \in T} \rho_{i,n} x_i, \quad (4a)$$

$$\text{s.t. } sw_i \leq t_{i,n} \leq ew_i - d_i, \quad (4b)$$

$$t_{i,n} + d_i + \Delta t_{i,n-j,m} \leq t_{j,m}, \quad (4c)$$

$$x_i \in \{0, 1\}, x_i \leq 1, \quad (4d)$$

where $\rho_{i,n}$ is the observation profit for target i at $t_{i,n}$; x_i a binary decision variable for target i , $x_i = 1$, denotes that target i is scheduled to be observed, otherwise $x_i = 0$; sw_i and ew_i the start and observation time of the VTW for target i ; d_i the duration of the OTW for target i ; and $\Delta t_{i,n-j,m}$ the attitude transition time between target i observed at $t_{i,n}$ and target j observed at $t_{j,m}$. Equation (4a) is the optimization objective function, which is to maximize the sum of collected profits; Equation (4b) represents the VTW constraint, which ensures that the observation of target i occurs within its VTW; Equation (4c) represents the attitude transition constraint, which guarantees that observing target j at $t_{j,m}$ is feasible after observing target i at $t_{i,n}$; Equation (4d) represents the value of the decision variable and the fact that a target can exist at most once in a single scheduling.

The observation profit $\rho_{i,n}$ ranges from 0 to 1, where 1 indicates that the conditions at $t_{i,n}$ allow us to achieve the highest possible image quality, and 0 denotes that the conditions are not appropriate for capturing the image at $t_{i,n}$. We formulate it as:

where GSD_{nadir} and $GSD_{i,n}$ are the GSD at nadir and for target i at $t_{i,n}$, respectively. As mentioned previously, the GSD increases as the target moves away from the nadir reaching its minimum at the nadir itself (see Fig. 2), i.e., the minimum GSD for each target is obtained in the middle of its VTW. Thus, the first term of the observation profit refers to image resolution. A small GSD value leads to a better resolution. The second term, $f_{i,n}(C_n^2(i, n), \delta_{i,n})$, represents the suitability of meteorological conditions.

V. ALGORITHM

The solution of the AEOSSP can be considered a sequential decision process in which the next action is selected based on the current graph, representing the state. Once the decision is made, the graph is updated so it includes only the last selected pair observation target i at a capture time n and the ones that are still feasible. This process is repeated until the resulting graph has only the last taken action, meaning that there are no more feasible actions.

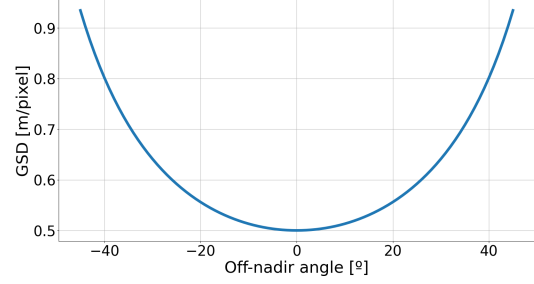


Fig. 2: Variation of GSD with respect to the off-nadir angle, assuming a GSD of 0.5 m/pixel at nadir.

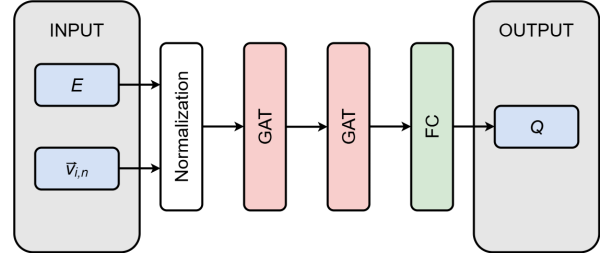


Fig. 3: GNN architecture.

Thus, we define a Markov decision process (MDP) $\langle S, A, T, R \rangle$, where: S is the state set represented by the graph; A the set of possible actions represented by the nodes in the graph; T the state transition function, which corresponds to the graph update based on the last selected action; and R the reward function, which corresponds to the observation profit when it is greater than zero, otherwise, it will correspond to a penalty.

The decisions that compose the final sequence of actions are made by a neural network. We make use of Graph Attention Networks (GAT) [11], a GNN structure that introduces the mechanism of attention to capture the most relevant characteristics of the graph. GATs are able to weight the relationships between the nodes of the graph based both on the features of the nodes and the edge structure.

Similar to [6], we propose a model with two single-layer GATs as embedding layers. We transfer the normalized features vector of each node $v_{i,n}$ along with the edges structure E in these layers obtaining the node embeddings. These embeddings, which contain meaningful information based on both node features and edge structure, are then passed through a fully connected layer that outputs a one-dimensional value representing the quality of a particular action. The proposed network architecture is shown in Fig. 3.

The parameters of the neural network are obtained by learning from batches of training data following a deep Q-learning (DQN) approach. In Q-learning, an agent aims to find the optimal policy that maximizes the long-term cumulative reward. For this, a state-action value Q_t is defined to describe the expected reward r_t of taking action a_t under state s_t at time t so that the agent can learn the optimal policy.

TABLE I: Simulation parameters.

Parameter	Value
d_i	0.15 s
l_{target}	5 km
δ_{max}	0.25
GSD_{nadir}	0.5 m/pixel
$C_n^2_{max}$	$5 \times 10^{-15} m^{-2/3}$
$\theta_{max}, \phi_{max}, \psi_{max}$	$45^\circ, 45^\circ, 90^\circ$
h_{sat}	600 km
ζ	98.6°
h_{clouds}	10 km
l_{clouds}	2 km
P_{clouds}	{0.4, 0.6}
$h_{C_n^2}$	20 km
$l_{C_n^2}$	10 km
$P_{C_n^2}$	{0.2, 0.4}
VTW duration	[18 - 185] s
Average observation period	{1623.79, 977.95} s
N	{40, 60, 80, 100}

Mathematically, this is expressed as:

$$Q_t(s_t, a_t) = (1 - lr)Q_t(s_t, a_t) + lr(r_t + \gamma \max_a Q_{t+1}(s_{t+1}, a)), \quad (5)$$

where γ is the discount factor that adjust the importance of future rewards over time and lr the learning rate. At each time step the agent takes an action a_t , observes the reward r_t , and the state is updated to s_{t+1} depending on s_t and a_t until the episode is over. An episode is defined as a complete sequence of interactions between the agent and the environment, starting from an initial state and ending when a specific termination condition is reached. The Q-table is updated with every time step t . In a DQN framework, a deep neural network is employed to estimate the state-action value Q_t . In our context, the agent is the AEOS; the state s_t the current graph at time t ; the action a_t the scheduled target based on s_t ; r_t the observation profit if it is greater than zero, otherwise it corresponds to a penalty; the next state s_{t+1} is the updated graph after selecting the action; the beginning of an episode corresponds to the initial graph with the virtual node and its termination condition is the exhaustion of the set of possible actions. We follow an ϵ -greedy policy: an exploration rate ϵ is defined, so that the agent choose a random action with a probability ϵ and the one that maximizes the expected reward with a probability $1 - \epsilon$. We define an initial exploration rate ϵ_0 that decays by a factor ϵ_{decay} with each episode until a minimum exploration rate ϵ_{min} is reached in order to favor exploration during the initial episodes. We use mean square error function to calculate the loss and the network parameters are updated according to stochastic gradient descent (SGD). The training process is shown in Algorithm 1.

VI. RESULTS

In order to simplify the problem, we make some assumptions. We assume that all the targets in the set have the same size, that can be captured in a single shot, and that the duration of the observation is the same for each target. We also set only three possible observation times for each target when using

Algorithm 1 DQN algorithm training

```

1: Input: Set of training episodes  $E$ ,  $\epsilon_0$ ,  $\epsilon_{decay}$ ,  $\epsilon_{min}$ ,  $\gamma$ ,
   training batch size  $batch_{size}$ 
2: Output: Network parameters
3: Initialize  $\epsilon = \epsilon_0$ ,  $memory \leftarrow \emptyset$  and DQN
4: for  $e$  in  $E$  do
5:   Set initial Graph  $G$  for episode  $e$ ,  $s_t = G$ 
6:   Get initial set of possible actions  $A_t$ 
7:    $done = False$ 
8:   while not  $done$  do
9:     if  $random(0,1) > \epsilon$  then
10:      Sample random action  $a_t$  form  $A_t$ 
11:     else
12:      Sample action  $a_t$  from  $A_t$  according to
        DQN( $s_t, a$ )
13:     end if
14:     Get reward  $r_t = R(s_t, a_t)$ 
15:     Update graph  $G$ ,  $s_{t+1} = G$  and set of actions  $A_t$ 
16:     if  $A_t$  is empty then
17:        $done = True$ 
18:     end if
19:     Store  $\{s_t, a_t, r_t, s_{t+1}, done\}$  in  $memory$ 
20:     Update state  $s_t = s_{t+1}$ 
21:     if  $length(memory) \geq batch_{size}$  then
22:       Sample random training  $batch$  from  $memory$ 
23:       for  $\{s_t, a_t, r_t, s_{t+1}, done\}$  in  $batch$  do
24:          $Q_t = DQN(s_t, a_t)$ 
25:         if not  $done$  then
26:            $Q_{t+1}^{max} = \arg \max(DQN(s_{t+1}, a))$ 
27:            $target = r + \gamma \cdot Q_{t+1}^{max}$ 
28:         else
29:            $target = r$ 
30:         end if
31:          $Loss(Q_t, target)$ 
32:         Update DQN using SGD
33:       end for
34:     end if
35:   end while
36:   if  $\epsilon > \epsilon_{min}$  then
37:      $\epsilon = \epsilon \cdot \epsilon_{decay}$ 
38:   end if
39: end for

```

TABLE II: Learning parameters.

Parameter	Value
ϵ_0	1
ϵ_{decay}	0.999
ϵ_{min}	0.01
γ	0.999
Learning rate	5×10^{-5}
$batch_{size}$	64
Number of training episodes	5000

the proposed model: at the beginning, in the middle, and at

the end of its VTW; and an initial satellite attitude of $\theta_0 = 0^\circ$, $\phi_0 = 0^\circ$, $\psi_0 = 0^\circ$. The simulation parameters are shown in Table I, while Table II displays the learning parameters. Code execution and training use an Nvidia A100 GPU with 1 TB of RAM. The algorithm and the simulator are implemented in Python and PyTorch 2.2.0 is used as learning framework.

The performance of the algorithm will be compared with two baselines: (1) **MaxResolution**, in which the observation time of each target is set to the middle of its VTW, i.e., when we get the best possible resolution for the image. The scheduling is decided according to this parameter and meteorological conditions are not taken into account; (2) **MaxTargets**, in which we aim to capture as many observation targets as possible. These are arranged in ascending order according to their VTW and those that are feasible are captured at their earliest observation start time [12]. Image resolution and meteorological conditions are not taken into account.

To evaluate the performance of both the proposed model and the baselines, four metrics will be used: the total observation profit obtained at the end of the episode, as described in Section IV, the precision, the percentage of discarded images, and the energy waste due to attitude maneuvers. We define the precision as follows:

$$\text{Precision} = \frac{N'_{sch}}{N_{sch}}, \quad (6)$$

being N_{sch} the total number of targets in the final scheduling and N'_{sch} the number of targets in the final scheduling whose observation profit is greater than zero. A higher precision value leads to a more efficient management of memory and energy resources, as it reduces both the number of discarded images and the corresponding attitude maneuvers required to capture them. The energy consumption is quantified in units of energy per unit of attitude transition time [1], so we can calculate the energy waste due to these actions.

A. Training

First, we train the neural network with instances of targets randomly generated of four different instance sizes: $N = 40, 60, 80$ and 100 targets. Thus, we obtain four different models depending on the size of the training instances. We consider an average observation period, i.e., the period in which the VTW of the targets are distributed, of 1623.79 seconds, and clouds and atmospheric turbulence are randomly distributed above the observation area according to $P_{clouds} = 0.4$ and $P_{C_n^2} = 0.2$ for each instance. Fig. 4 shows the average loss per training batch for the case of the training with instances of 40 targets, where a rapid decay and convergence can be observed. We also test the four trained models against instances of size $N = 40, 60, 80$ and 100 targets and generated in the same conditions as the training (200 instances each). Results are displayed in Fig. 5. Although precision does not vary significantly, the model trained with instances of 40 targets gets the highest observation profit in all cases. Therefore, this model will be the one used in the following evaluations.

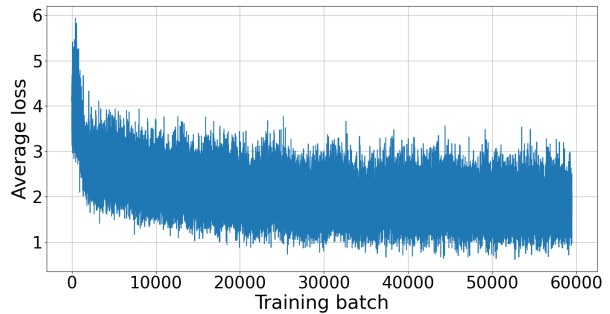


Fig. 4: Average loss per training batch.

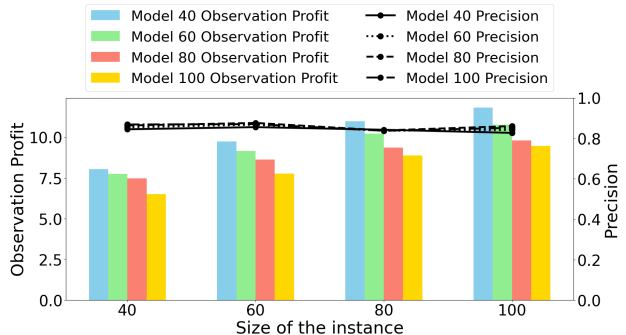


Fig. 5: Observation profit and precision for different graph sizes ($N = 40, 60, 80, 100$) and trained model.

B. Model Performance

We consider four different cases to test the performance of the proposed model and the baselines: (1) instances generated under the same conditions as the training instances; (2) the average observation period is reduced while maintaining the number of targets per instance, so that the decision-making process becomes more critical; (3) more severe meteorological conditions are considered, i.e., higher P_{clouds} and $P_{C_n^2}$ values; (4) a combination of (2) and (3), representing the most challenging case. Like in the model comparison, tests consist of 200 instances.

Fig. 6a shows the results for the case (1). The observation profit obtained by the model only surpasses the MaxTargets baseline in the 100-target instance and ranges from 78% to 99% of the baseline values in all other cases, but the precision values are significantly improved, increasing from approximately 52% to 85%. This results in a significantly more efficient memory utilization, as the number of discarded images due to cloud coverage or atmospheric turbulence decreases by 68.75%, and a reduction of a 65% and 75% of energy waste from attitude maneuvers with respect to the MaxResolution and MaxTargets baselines is achieved, respectively.

For case (2), we consider an average observation period of 977.95 seconds. The results are displayed in Fig. 6b. In this case, the observation profit obtained by the predicted scheduling outperforms the one obtained for the baselines except for the 80- and 100-target instances for the MaxResolution baseline. Furthermore the number of discarded images is reduced by 67.65% and the energy waste by 57% and 69%

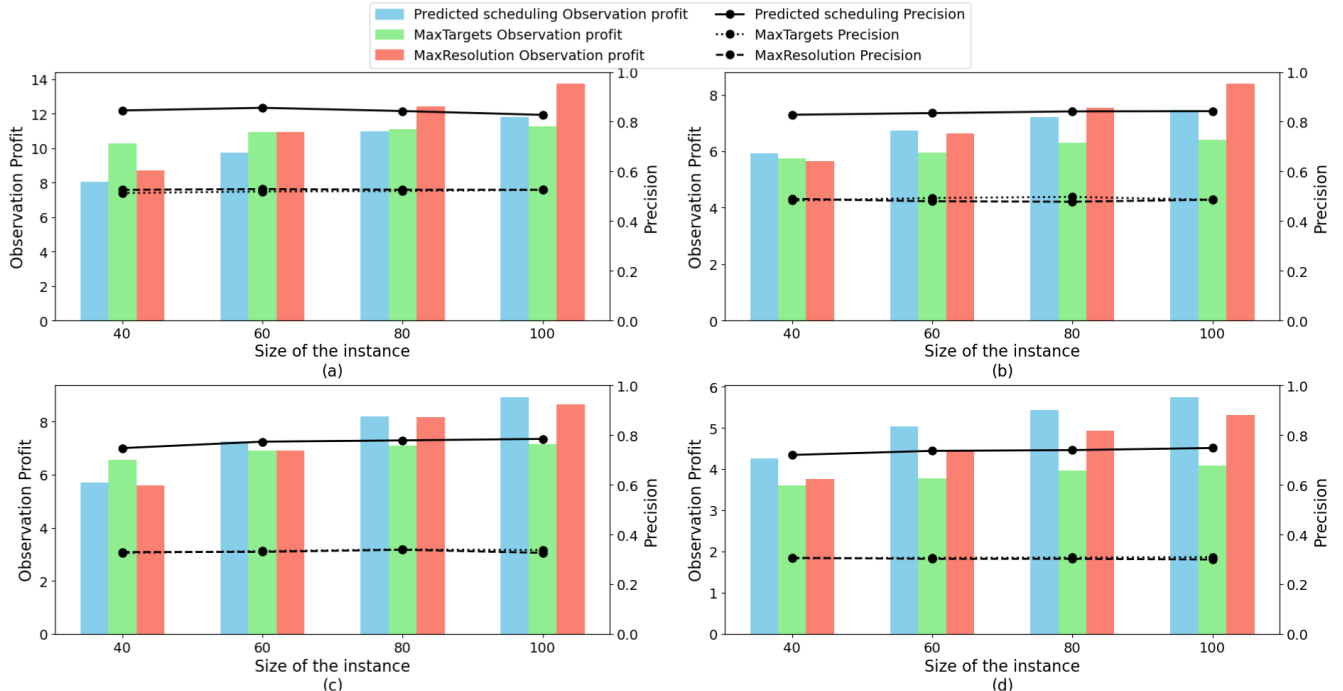


Fig. 6: Observation profit and precision. (a) Average observation period = 1623.79 seconds, $P_{clouds} = 0.4$, and $P_{C_n^2} = 0.2$. (b) Average observation period = 977.95 seconds, $P_{clouds} = 0.4$, and $P_{C_n^2} = 0.2$. (c) Average observation period = 1623.79 seconds, $P_{clouds} = 0.6$, and $P_{C_n^2} = 0.4$. (d) Average observation period = 977.95 seconds, $P_{clouds} = 0.6$, and $P_{C_n^2} = 0.4$.

with respect to the MaxResolution and MaxTargets baselines, respectively.

Fig. 6c illustrates the results for case (3). We consider $P_{clouds} = 0.6$ and $P_{C_n^2} = 0.4$. Similarly to the previous case, the observation profit obtained by the model is greater than the one obtained by the baselines, except in the 40-target instance for the MaxTargets baseline. We also achieve a reduction of 64.2% in the number of discarded images and 66% and 78% of wasted energy with respect to the MaxResolution and MaxTargets baselines, respectively.

Finally, in case (4) we consider an average observation period of 977.95 seconds, $P_{clouds} = 0.6$, and $P_{C_n^2} = 0.4$. Fig. 6d shows the results. The proposed model achieves a higher observation profit in all cases and reduces the number of discarded images by 61.4% and the wasted energy by 55% and by 69% with respect to the MaxResolution and MaxTargets baselines, respectively.

Thus, we can conclude that the proposed model presents a good management of memory and energy resources. Furthermore, it has a great scalability capacity, since good results are obtained in instances of very different sizes, and outperforms the considered baselines in complex cases, highlighting the importance of an accurate decision making process.

VII. CONCLUSIONS

We propose a DRL approach for the AEOSSP with time-dependent profits considering the impact of the cloud occlusion, atmospheric turbulence and image resolution in order to improve the management of the energy and memory resources. We model the AEOSSP as a directed graph representing

the current state that is dynamically updated according to the last action and propose a neural network trained in a DQN framework that leverages the potential of the GAT to decide the best next possible action. The results show that the proposed model reduces the number of discarded images by $> 60\%$ and energy waste from attitude maneuvers by up to 78%. Furthermore, it outperforms the baselines considered in challenging cases in terms of observation profit.

Future work will do the integration into the operation of an EO satellite network with a joint optimization of the image acquisition process, data processing and communication, enabling more efficient use of the resources of the satellite and the overall system. For this, we will consider a multi-satellite scenario and extend the formulation of the observation profit.

REFERENCES

- [1] X. Wang, G. Wu, L. Xing, and W. Pedrycz, "Agile Earth Observation Satellite Scheduling Over 20 Years: Formulations, Methods, and Future Directions," *IEEE Systems Journal*, vol. 15, no. 3, p. 3881–3892, Sep. 2021. [Online]. Available: <http://dx.doi.org/10.1109/JSYST.2020.2997050>
- [2] G. Yi, C. Han, Y. Chen, and W. Xing, "Mission Re-planning For Multiple Agile Earth Observation Satellites based on Cloud Coverage Forecasting," *IEEE Journal of Selected Topics in Applied Earth Observations and Remote Sensing*, vol. PP, pp. 1–12, 2021.
- [3] L. C. Andrews and R. L. Phillips, "Laser beam propagation through random media," *Laser Beam Propagation Through Random Media: Second Edition*, 2005.
- [4] W. Yi *et al.*, "Comprehensive Evaluation of the GF-4 Satellite Image Quality from 2015 to 2020," *ISPRS International Journal of Geo-Information*, vol. 10, no. 6, 2021. [Online]. Available: <https://www.mdpi.com/2220-9964/10/6/406>
- [5] R. S. Sutton and A. G. Barto, *Reinforcement Learning: An*

Introduction, 2nd ed. The MIT Press, 2018. [Online]. Available: <http://incompleteideas.net/book/the-book-2nd.html>

- [6] J. Chun, W. Yang, X. Liu, G. Wu, L. He, and L. Xing, "Deep Reinforcement Learning for the Agile Earth Observation Satellite Scheduling Problem," *Mathematics*, vol. 11, no. 19, 2023. [Online]. Available: <https://www.mdpi.com/2227-7390/11/19/4059>
- [7] H. Chen, S. Peng, C. Du, and J. Li, *Earth observation satellites : task planning and scheduling*, 1st ed. Singapore: Springer Nature Singapore, 2023.
- [8] B. Soret *et al.*, "Semantic and goal-oriented edge computing for satellite Earth Observation," 2024. [Online]. Available: <https://arxiv.org/abs/2408.15639>
- [9] G. Peng, R. Dewil, C. Verbeeck, A. Gunawan, L. Xing, and P. Vansteenwegen, "Agile earth observation satellite scheduling: An orienteering problem with time-dependent profits and travel times," *Computers & Operations Research*, vol. 111, pp. 84–98, 2019. [Online]. Available: <https://www.sciencedirect.com/science/article/pii/S0305054819301510>
- [10] X. Liu, G. Laporte, Y. Chen, and R. He, "An adaptive large neighborhood search metaheuristic for agile satellite scheduling with time-dependent transition time," *Computers & Operations Research*, vol. 86, pp. 41–53, 2017. [Online]. Available: <https://www.sciencedirect.com/science/article/pii/S0305054817300977>
- [11] P. Veličković, G. Cucurull, A. Casanova, A. Romero, P. Liò, and Y. Bengio, "Graph Attention Networks," 2018. [Online]. Available: <https://arxiv.org/abs/1710.10903>
- [12] C. Pralet and G. Verfaillie, "Time-dependent Simple Temporal Networks: Properties and Algorithms," *RAIRO - Operations Research*, vol. 47, no. 2, p. 173–198, 2013.